INFRARED SUBMILLIMETER AND RADIO ASTRONOMY RESEARCH AND ANALYSIS PROGRAM

Contract NCC2 1012

Final Report

For the Period: 1 December 1997 through 31 May 2000

Principal Investigator
Dr. Wesley A. Traub

June 2000

Prepared for

National Aeronautics and Space Administration
Ames Research Center
Moffett Field, CA 90435-1000

Smithsonian Institution
Astrophysical Observatory
Cambridge, Massachusetts 02138

The Smithsonian Astrophysical Observatory
is a member of the
Harvard-Smithsonian Center for Astrophysics

INFRARED SUBMILLIMETER AND RADIO ASTRONOMY RESEARCH AND ANALYSIS PROGRAM

FINAL REPORT

For the period 1 December 1997 through 31 May 2000

Principal Investigator: Dr. Wesley A. Traub

This program entitled "Infrared Submillimeter and Radio Astronomy Research and Analysis Program" with NASA-Ames Research Center (ARC) was proposed by the Smithsonian Astrophysical Observatory (SAO) to cover three years. Due to funding constraints only the first year installment of $18,436 was funded, but this funding was spread out over two years to try to maximize the benefit to the program.

During the tenure of this contact, the investigators at the SAO, Drs. Wesley A. Traub and Nathaniel P. Carleton, worked with the investigators at ARC, Drs. Jesse Bregman and Fred Witteborn, on the following three main areas:

1. Rapid scanning

SAO and ARC collaborated on purchasing and constructing a Rapid Scan Platform for the delay arm of the Infrared-Optical Telescope Array (IOTA) interferometer on Mt. Hopkins, Arizona. The Rapid Scan Platform was tested and improved by the addition of stiffening plates which eliminated a very small but noticeable bending of the metal platform at the micro-meter level. The platform has since seen heavy usage on an essentially daily basis, and has performed extremely well on our classical Michelson beam-combination infrared table.

2. Star tracking

Bregman and Witteborn conducted a study of the IOTA CCD-based star tracker system, by constructing a device to simulate star motion having a specified frequency and amplitude of motion, and by examining the response of the tracker to this simulated star input. A key result of this research is that the system gain was found to be optimum at a value well below that which we originally considered to be correct (roughly a factor of two lower). We now believe that this result can be readily explained by the effect of the finite time delay involved in the read-out cycle of the CCD, and the subsequent computation cycle, all prior to the application of a correction signal to the piezo-mirror which is used to compensate for the atmospherically-induced instantaneous tilt of the incoming star-light beam. This new understanding of the system has led us to propose that a second-generation star tracker should be built, based on the more rapidly responding avalanche photo diode (APD) technology. The only impediment to implementation is that APDs are significantly more expensive than our current CCD detectors.

3. Fringe tracking.

ARC, and in particular Dr. Robert Mah, developed a fringe-packet tracking algorithm, based on data that Bregman and Witteborn obtained on IOTA. The algorithm was tested in the laboratory at ARC, and found to work well for both strong and weak fringes. The next step in this program occurred when Dr. Sebastien Morel came to work at IOTA as a post-doctoral fellow, under a one-year French government sponsorship. Morel's first task at IOTA was to travel to ARC and meet with Traub, Bregman, and Mah, to discuss the possibility of transferring this algorithm from the laboratory to a real-time application at the IOTA interferometer. Morel was successsful in adapting a simplified version of the algorithm to a laptop computer at IOTA, which was then connected to a control computer to command the Rapid Scan Platform. The implementation of the algorithm allowed fringe-packet centroid compensation at a rate of ten times per second. A number of computer interconnection problems slowed the full application of this

research, but the basic principle was demonstrated successfully. Subsequently, Morel was able to spend a second year at IOTA, this time under NASA sponsorship, with the goal of completing the application of the control algorithm. Morel is currently nearing the mid-point of this second year. Since a major activity at IOTA this year is the installation of a new, real-time, control system, which will include within its structure the entire fringe-tracking measurement and command algorithm, Morel has also become an active player in the coding of the control system software. The new system will be a huge improvement over the current system, from the point of view of the fringe-tracking algorithm, in that all computations and commands will take place in a single real-time computer, thus obviating the need for communications between different computers and avoiding the associated time delays. The new system will also be capable of controlling three telescopes at once, thus allowing us to make phase-closure measurements with IOTA, and for this purpose the fringe packet tracking capability is an absolute requirement. We recently reported results from this program at the Munich meeting of the SPIE in March 2000. Preprints of two relevant papers from this meeting are attached as appendices to this report. The papers are "The Third Telescope Project at the IOTA Interferometer" by Traub, Carleton, Bregman, et al., and "Fringe-tracking Experiments at the IOTA Interferometer" by Morel, Traub, Bregman, Mah, and Wilson.

Summary

All three of the above elements are currently being brought together in a single real-time control system for IOTA which will enable phase-closure measurement experiments to begin within the next year. The support of the current grant has been crucial to progress in this direction. We look forward to the coming year, in which we hope to see the culmination of our efforts to establish phase-closure capability at IOTA. Collaboration will continue with ARC in the development and evolution of the IOTA control system.

The Third Telescope Project at the IOTA Interferometer

Wesley A. Traub[a], N.P. Carleton[a], J.D. Bregman[b], M.K. Brewer[c], M.G. Lacasse[a], P. Maymounkov[a], R. Millan-Gabet[a], J.D. Monnier[a], S. Morel[a], C. Papaliolios[a], M.R. Pearlman[a], I.L. Porro[a], F.P. Schloerb[c], K. Souccar[c]

[a]Harvard-Smithsonian CfA, 60 Garden St., Cambridge, MA 02138
[b]NASA Ames Research Center, MS 245-6, Moffett Field, CA 94035
[c]Physics and Astronomy Dept., Univ. of Massachusetts at Amherst, Amherst, MA 01003

ABSTRACT

The third telescope project to enable phase-closure observations at the IOTA interferometer is well underway, and is anticipated to be completed later this year. For this project, we present the main technical improvements which we have already made or expect to make, including a new VxWorks control system, improved star acquisition cameras, improved siderostat and primary mirror supports, five-axis control of the telescope secondary mirrors, automated control of the long delay line, trihedral retroreflectors, three-beam combination, the PICNIC camera, and fringe packet tracking.

Keywords: Interferometer, IOTA

1. INTRODUCTION

The Infrared Optical Telescope Array (IOTA) began scheduled operation in 1995, with two 0.45 m telescopes, and baselines up to 38 m. At the present time (1999-2000), a 3rd telescope and siderostat have been installed at IOTA, and the corresponding optics have all been polished and silver coated, and are either installed or nearly so. Likewise, the relay optics are mounted and ready to be installed. Three-beam operation is planned for late 2000.

An overview of progress and scientific results through 1998 was given in Traub.[1] Current progress and further scientific results are given elsewhere in this volume by Berger,[2] Hofmann,[3] Kervella,[4] Mennesson,[5] Millan-Gabet,[6] and Morel.[7]

In the present paper we outline some of the key projects currently underway at IOTA, in addition to those just mentioned above. The results here are essentially a progress report, since most of these projects are still in development.

2. VXWORKS CONTROL SYSTEM

2.1. Introduction

The goal of a telescope Monitor and Control system is to provide an efficient computing environment for monitoring, control, and data acquisition. The system should provide users with tools to compose observing plans, to submit them for execution, to monitor their execution in real time, to monitor the data generated by the instruments in real time, and to record and archive scientific and engineering data. The system should also provide interfaces to integrate new instruments and to host visiting instruments; and it must be capable of incorporating user preferences.

The basic architecture and design principles for the IOTA Monitor and Control system are based on work being carried out in support of the Large Millimeter Telescope (LMT) project at the University of Massachusetts. IOTA is making use of the LMT development effort, which is designing an open architecture system that is implemented using existing components developed at other observatories wherever possible.

Further author information: (Send correspondence to W. Traub).
Email: WAT: wtraub@cfa.harvard.edu ; NPC: ncarleton@cfa.harvard.edu ; JDB: jbregman@mail.arc.nasa.gov ;
MKB: brewer@fcrao1.phast.umass.edu ; MGL: mlacasse@cfa.harvard.edu ; PM: maymounk@fas.harvard.edu ;
RMG: rmillan@cfa.harvard.edu ; JDM: jmonnier@cfa.harvard.edu ; SM: smorel@cfa.harvard.edu ;
CP: cpapaliolios@cfa.harvard.edu ; MRP: mpearlman@cfa.harvard.edu ; ILP: iporro@cfa.harvard.edu ;
FPS: schloerb@astro.umass.edu ; KS: souccar@astro.umass.edu

2.2. Description of the Monitor and Control System

The IOTA monitor and control system comprises of a set of modules with control and data flows among them. It is illustrated in Figure 1. At the front end of the system is an observing tool that is used to compose observing plans. These plans are in turn submitted to a finite state machine controller to be executed according to a predefined or dynamically determined schedule. The same observing tool is used to run the telescope interactively for scientific or engineering purposes.

While observing commands are being executed, the state of the system is monitored by the user, and scientific and engineering data are collected. An observing simulator is provided to test the validity of observing programs.

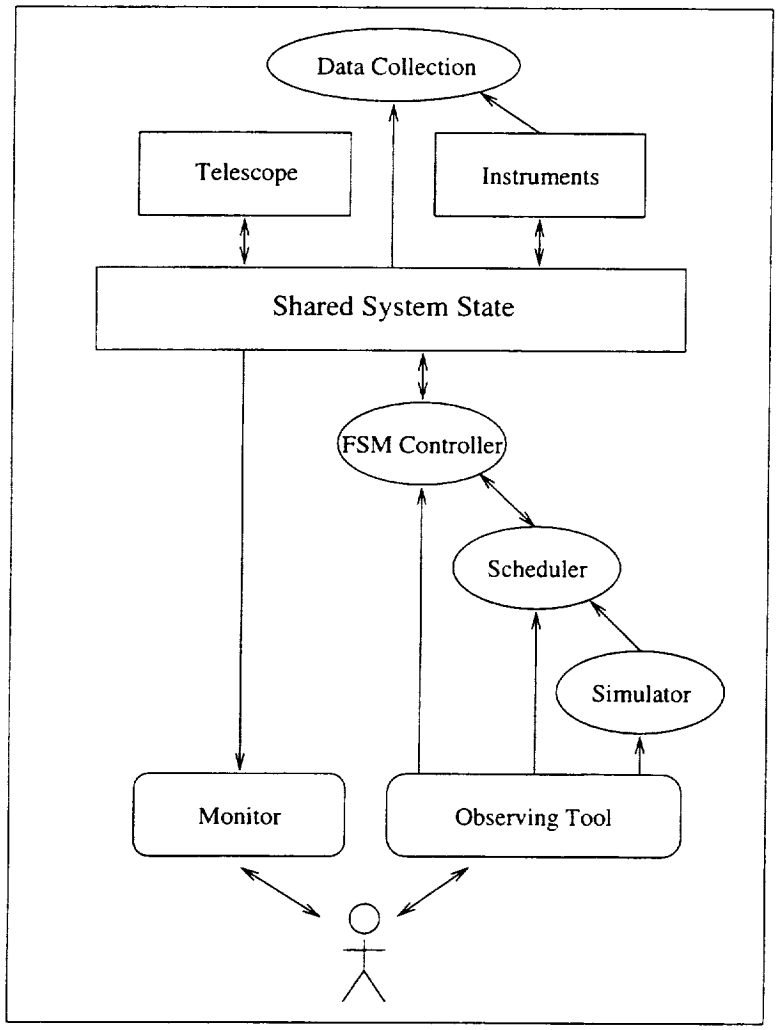

Figure 1. The IOTA Monitor and Control System

2.2.1. Observing Tool

The observing tool provides the means for the user to input desired commands to the system and to execute them on line. These commands can also be saved in a file to be scheduled for later execution.

The user creates a science program that may include one or more observing programs. Each observing program must contain scheduling constraints, target positions, a science instrument, and a data collection method.

In turn, the observing tool generates commands to control the different subsystems based on the science program composed by the user. The generated commands are implemented using a keyword-value pair method to set the

parameters of each subsystem. Expert users may choose to generate the observing commands by hand to short cut this process.

Ultimately, the project would like to modify Gemini's observing tool to be used for the IOTA and the LMT. In the mean time, we have built a web-based tool that mimics the functionality of Gemini project's observing tool to define science programs.

2.2.2. Scheduler

A queue scheduler schedules the execution of science programs according to their priorities and meteorological conditions. However, this does not preclude the system from accepting direct commands when it is in manual scheduling mode.

2.2.3. FSM Controller

A finite state machine (FSM) controller translates the observing programs into desired system states. It steps through the science program and executes each command while monitoring the state of the system.

2.2.4. Monitoring

The purpose of on-line system monitoring is to provide a running check on data integrity and proper system operation by displaying the state of the system to the user. The monitoring system provides real-time access to the observation state, telescope state, instrument states, etc. The initial implementation of the monitoring system uses Java software developed at the Owens Valley Radio Observatory by Steve Scott.

2.2.5. Data Collection and Processing

Data collection is the final outcome of an observing program. Data from instruments is tagged with telescope and system states and saved to disk for further processing. A quick-look data display, and some degree of quick analysis, should be provided.

2.2.6. Observing Simulator

The observing simulator is designed to test observing programs and train and familiarize observers with the telescope system. It provides the same exact functionality as the real system and can be run in real time, faster than real time, or single stepped through a debugging program.

2.3. Architecture of the Monitor and Control System

The complexity and requirements of the Large Millimeter Telescope necessitate a real-time distributed processing approach. Therefore, the LMT monitor and control system is being implemented as a distributed system consisting of independent modules running on multiple computers. The LMT Project has selected replicated shared memory to provide the interconnection among the multiple processes running on the different computing systems. This choice eliminates the large overhead associated with inter-process communication and minimizes real-time communication dependencies between subsystems. The initial implementation of the IOTA system will be far simpler than the LMT system and will probably be handled by one or more processors using shared memory in a single VME crate to provide the interconnection among the multiple processes running on the system.

3. IMPROVED STAR ACQUISITION CAMERAS

Each telescope at IOTA has a commercial CCD camera mounted near the back of the primary mirror, pointing perpendicular to the telescope axis, and illuminated by the 10-times reduced telescope beam from the secondary mirror via a remotely-controlled flip-in mirror. We recently installed new cameras which are an improvement over our previous ones in two aspects: the sensitivity is better, and the integration time can be selected. The new cameras are Panasonic WV-BP-550 black and white CCD cameras. The lens is a Fujinon f/1.2 zoom lens, which we set to its maximum focal length of 75 mm. This combination gives approximately 2 arcsec pixels on the sky, and about 15 arcmin field of view.

We also installed a Panasonic "looping switch" box and a controller, giving us the ability to display up to 8 camera inputs, either one at a time on a single monitor, or simultaneously on 1 monitor per camera. The controller

has many other functions, but the one which is most important to us is the ability to control the integration time, from a normal fast framing rate of 30 frames/sec, to a slow rate of about 1 frame/sec, in 6 selectable steps.

At the normal rate we can now easily see a $V = 12$ magnitude star, whereas with our previous cameras a $V = 12$ star was only barely visible against the background noise. Slowing the frame rate allows even fainter stars to be seen easily, but we find that the normal rate is adequate and comfortable for almost all our current work.

4. IMPROVED SIDEROSTAT AND PRIMARY MIRROR SUPPORT

In a recent study of the optical quality of the IOTA system[8] we found that the measured visibilities in the visible and infrared were approximately consistent with the known sources of wavefront degradation. Ranking the expected main sources of wavefront degradation, we found that 3 of them dominated: the wavefront curvature from atmospheric turbulence, the servo system time constant, and the flatness of the relay optics surfaces, approximately in rank order.

We intend to address the first 2 sources in the future. However we recently attempted to reduce a part of the flatness error by improving the mounting technique used for the 2 large optical elements in our train, the siderostat and the telescope primary mirror. These are approximately 45x68 cm and 45 cm diameter, respectively, and each is about 7.6 cm thick, i.e., about 1/6 times the beam diameter.

The primary mirror points downward toward the siderostat mirror, with its optical axis inclined by 30° below the horizontal. Most of the weight of the mirror is supported by 2 nominally low-friction pads along the bottom edge of the mirror. There are also 3 hard points on the back of the mirror, and each is flanked closely by 2 springs which pull the mirror back against the hard points.

The improvement we have recently made is to incorporate high precision ball slides into the 2 lower edge supports to reduce friction. The friction is now small enough that the springs on the back of the mirror easily keep the mirror held snugly against its 3 back-plane hard points. Previously, the edge friction force was sometimes greater than this spring force, and the mirror would occasionally slip away from its lower hard point, thereby misaligning the telescope slightly. The larger edge friction also could have contributed to a bending of the mirror, which we are now sure is negligibly small.

We also installed a lifting spring on each primary mirror, pulling upward at a 30° angle from the vertical, on the top edge of the mirror, along a line perpendicular to the optical axis. This spring is gauged to oppose the tendancy of the top edge of the mirror to droop forwards.

The siderostat flat rests on 3 hard points on its back side, and is restrained from slipping in the plane of the mirror surface by a pair of tangent arms. The original design included 6 air bags on the back of each siderostat mirror, which could be inflated with air and which would then remove some of the weight of the mirror from the 3 hard points. However we found it difficult to control the air pressure sufficiently well to provide a nominal lifting force, without floating the mirror completely free of the hard points, so in practice we have not used the air bag system. However we recently purchased a custom air bag which covers much of the back area of the mirror, and will more easily take up the irregularities of spacing between the mirror and the cradle back. We expect to install and test this device in the near future.

5. FIVE-AXIS CONTROL OF THE TELESCOPE SECONDARY MIRRORS

The original design of the IOTA secondary mirror mounts included a 3-axis translation stage immediately behind the secondary mirror, adjustable by manual micrometer screws, and a tip-tilt adjustment capability of the entire spider assembly via coarse screw threads at the ends of the spider arms. Aside from this adjustment capability, the mechanical spacing of the primary and secondary has been, and will continue to be, controlled through a path that is nominally thermally invariant, using 3 ceramic rods and appropriate metal connection.

However this original mechanism of adjustment of the secondary with respect to the primary proved to be awkward in practice, in part because the tip-tilt also had a component of translation, and in part because the adjustments were done manually at the telescope, whereas the sensing of the wavefront was done interferometrically in the laboratory, making communication between the people at either end difficult.

We recently made 2 major changes to this system, with the hope of making this adjustment easier to carry out.

The first change is that we replaced the secondary mirror's commercial 3-axis translation stage with a compact 5-axis stage of our own design. The new stage uses New Focus Picomotors for motion control. These devices have

step sizes of about 1/40 wavelength, and they are remotely commandable. Three Picomotors are mounted directly behind the secondary mirror, with their axes nominally parallel to the telescope optical axis. Thus a motion of any one of these motors produces a tip or tilt action of the secondary, plus a small translation. The action of all 3 together produces a focus change. In our design these 3 motors are mounted on a plate which can be rotated slightly about 2 axes perpendicular to the optical axis, thus producing a translation of the secondary, perpendicular to the focus direction. The pivot axes are supported by flexure elements from Lucas Aerospace. The combination gives complete 5-axis control.

After building these units, and permanently installing them on the telescopes, we discovered 2 problems which we are still working to resolve. One problem is that the motors have significantly different step sizes from motor to motor, due in part to the different axial loading forces on each screw, caused by differences in tension of the pre-load springs used in our design. A second problem is that each motor has a significantly different step size in the forward and reverse direction, a factor which seems to be independent of axial load or friction.

(We also discovered a third problem, which we have since solved. In an effort to avoid several mechanical interferences, we removed the knurled knob attached to the end of several of our Picomotors. The knob is used to manually turn the Picomotor screw, and we thought we could work without it present. It turns out that the inertia of the knob is crucial to the successful operation of a Picomotor, and to restore nominal operability we had to replace the knobs with little flywheels of comparable inertia, tailored to our spatial constraints.)

From our limited experience it seems that the individual step size differences can probably be calibrated to some extent, but we have not yet done this. Calibration will be required in order to make our 5-axis stages easier to use. An additional step will then be to write the remote command program in such a way that it can carry out combined motions of the motors to give focus, orthogonal translation, and tip-tilt.

The second change was to build a simple telescope alignment interferometer for use at the telescope, instead of having the interferometer in the distant laboratory. The advantage here is simply that the distance from the secondary to the test interferometer is now only about 3 m, as opposed to about 30 m to the lab, so that a small change of the secondary mirror tilt or position will not cause the reflected laser beam to become lost. The system works by sending an expanded parallel beam of laser light out from the lab, passing it through a beamsplitter near the telescope, sending the reflected beam to a flat mirror and back to the beamsplitter, and sending the transmitted beam to the secondary, primary, siderostat flat (tilted to autocollimation position), back to the primary, to the secondary, and finally to the beamsplitter. Fringes in the combined output beam indicate telescope misalignment. We adjust the secondary to eliminate the fringes, as much as possible. Residual errors amount to roughly one fringe, due in part to flatness errors, and perhaps in part to mounting errors in the large optics, as discussed above. Operationally, the fringes are easy to see by eye, and the adjustment of the secondary is relatively rapid, although due to the problems mentioned above with motor step sizes, at present we are making these adjustments by manually turning the motor screws, which is adequate from a sensitivity point of view.

6. AUTOMATED CONTROL OF THE LONG DELAY LINE

In the original design of IOTA, we split the beam from a single laser to control both the short and long delay lines, which sufficed for a 2-telescope interferometer. In the current design, we have 3 telescopes, and must therefore have at least 2 sets of short and long delay lines. An additional requirement is that we want to have the long delay position continuously monitored, whereas in the original system we shuttered the long delay laser beam during star observations, because it scattered light into the science beam.

The new design uses one laser split to control the 2 short delay lines, and a second laser split to control the 2 long delay lines. In addition, the long delay laser has been moved to the far end of the delay line, so that the laser beam no longer runs close to the science beam. The laser retroreflector has been moved from the front of each long delay cart to the back of the cart. Fine control of the laser beam direction is controlled by a steering flat mounted on a 2-axis Picomotor mount, which gives adequate directional control.

The long delay laser is an HP-5517A. We also use HP optics, receiver heads, and pulse counting electronics boards, the latter being installed in a dedicated computer. The laser and computer are located in a small hut at the extreme north-east end of the long delay line. The laser beams are passed into the vacuum tank via 2 windows mounted in the end cap of the long delay vacuum pipe.

The remote computer communicates via UDP packets, once per second, in a client-server relationship, with a control computer in the laboratory. Several modes of operation are available. The long delay cart can be commanded to home, using an opto-interrupter switch, giving an accuracy of about 10 μm, which is adequate. The cart can be moved to a desired position within 1 mm or so, using open-loop commands to a stepping motor that drives a steel cable pulling the cart. The actual position achieved is determined from the laser, and the offset from the desired position is communicated to the short delay line, which compensates accordingly.

The cart has a slew speed of 20 cm/sec, which means that long delay reconfigurations can be carried out relatively quickly. Since the position is continuously monitored, we have the capability to correct for small thermal changes throughout the night.

The new system is thus a big improvement over the original system, which required a sequence of relatively clumsy and slow operations each time the cart needed to be moved. The only remaining issues which we need to address in the near future are the straightness of the track, which causes the laser beam to lose strength (but not to fail) at one particular segment of the track, and the scattered laser light, which needs some basic baffling to keep it from leaking past the cart and into the vicinity of the science beam.

7. TRIHEDRAL RETROREFLECTORS

The original IOTA design uses dihedral (2 flats at 90°) reflectors on both the long and short delay lines. About one year ago we began to fabricate trihedral (3 flats at 90° to each other) reflectors, also known as hollow cube corners, to replace the dihedrals.

Our reason for wanting trihedrals is that they are immune to tilt errors. Our long delay line track is straight to an accuracy of only about 0.01 cm or so, which means that every time the dihedral is moved to a new position on the track, the dihedral must also be corrected in yaw angle by roughly 100 arcsec. We routinely do this operation manually, taking as our visual reference a Maglite bulb which is flipped onto the nominal optical axis near the telescope. We then send a modulated infrared signal to a battery-driven motor on the cart, controlling the direction and speed of rotation of the motor; the motor drives a micrometer screw which changes the yaw angle of the dihedral. This ensures that the science beam stays nominally centered on the relay optical elements, and enters the beam combination area without vignetting. Fine-scale correction is supplied automatically during star observations by the star tracker system.

We designed a trihedral mirror and mount subsystem, and fabricated the mechanical and optical components. The trihedral comprises an upper mirror unit and a lower mirror unit, both held in a stiff aluminum frame with appropriate fine-pitch adjusting screws. The lower mirror unit is a single flat. The upper mirror unit is a pair of flats, held at 90° by a diagonal brace. The mirrors are Astrositall, and the brace is ULE. The mirrors are 1/20 wave peak to valley and silver coated (Denton FSS-99), similar to the other flat relay mirrors in IOTA.

Due to space constraints, the star beam is centered on the vertex line between the two upper mirror halves. In order to introduce no more than a 1/20 wave peak to valley additional wavefront error from the error in the 90° angle between these mirror halves, the tilt of the reflected wave segments must be no more than 0.4 arcsec. To achieve this accuracy we inserted the mirror segment assembly in one arm of an interferometer, and adjusted the angle until straight fringes were achieved.

We then glued the segments in place using the diagonal brace and 2 small supporting right-angle prisms along the back edge of the hinge line between segments. The glue is an ultra-violet light setting cement (Norland 61) commonly used for optical assemblies. We found that as it cured, over a time interval of roughly 10 to 100 sec, depending upon the UV light intensity, the cement changed dimension by a small but non-negligible amount. The result was that our included angle became acute, by an amount sufficient to make the straight-fringe interferogram turn into a chevron shape, with nominally one fringe of error at the edge of the assembly.

Subsequent inquiry suggests that this cement and others like it all experience a small shrinkage when cured, a behavior which is consistent with the observed change of angle. We have tried many variations of this experiment and always end up with the same or worse result. We are sure that the problem arises because of glue shrinkage. Other effects, such as thermal drifts and heating of the glass materials by the UV lamp, are demonstrated to be much smaller.

We believe that the mirrors must be rigidly bonded by cement in order to preserve the 1/20 wave criterion, and in particular that they cannot be held by an external metal framework. Our failure to achieve the desired accuracy

is a design challenge for the future. But in order to continue to make progress with the third telescope project, we have decided to abandon trihedrals for the near future, and instead use the dihedrals which have served us well for several years now, albeit with the nuisance of having to make a yaw correction every time the long delay mirror is moved.

8. THREE-BEAM COMBINATION

We have several paths that we can follow to achieve the 3-beam combination required for phase-closure measurements. Each of the paths mentioned here is currently being pursued.

For the infrared JHK bands we will build a classical Michelson beam-combiner assembly, using flat-plate combiners. For the infrared H band we will install an integrated optics beam combiner, currently being developed at Grenoble Observatory[9]; this project will be led by J.-P. Berger. For the visible, we are starting to experiment with visible-wavelength single-mode fibers, first for 2 beam combination, and later with 3 beams. These projects will be reported in future publications.

9. PICNIC CAMERA

Our project to upgrade our NICMOS3 camera[10] to a lower read-noise PICNIC chip is well underway, but not yet complete. We plan to build 2 such detector units, so that the second can be used as an infrared star tracker for sources with low visible-wavelength signals.

10. FRINGE PACKET TRACKING

Progress toward fringe tracking at IOTA is reported in this volume by Morel.[7] The basic idea is that we are trying to merely keep the interference fringe packet centered in our scan window, to an accuracy of about one wavelength, for the purpose of being able to have the fringe packets in the 3-telescope system all be recorded at nearly the same instant of time. It is not necessary to control the piston to much greater accuracy for phase closure. The packet tracker has been successfully tested in preliminary experiments at IOTA, and it is currently being reformulated for inclusion in the VxWorks control system, where its implementation will be much simpler than is presently possible.

We are grateful to NASA for funding (NAG5-4900) the hardware required for the 3rd telescope upgrade at IOTA, and for supporting the fringe-packet tracking work for IOTA at SAO and NASA-Ames. We also gratefully acknowledge ongoing institutional support from the Smithsonian Astrophysical Observatory and the University of Massachusetts at Amherst.

REFERENCES

1. W. A. Traub, "Recent results from the IOTA interferometer," in *Proc. SPIE 3350: Astronomical Interferometry*, R. D. Reasenberg and J. B. Breckinridge, eds., p. 848, 1998.
2. J.-P. Berger, F. Malbet, R. Millan-Gabet, W. Traub, and M. Colavita, "Insights in the nature of the sub-AU circumstellar environment of FU Orionis," in *Proc. SPIE 4006: Interferometry in Optical Astronomy*, P. Lena and A. Quirrenbach, eds., SPIE, 2000.
3. K. Hofmann, T. Bloecker, V. C. du Foresto, M. Lacasse, S. Morel, B. Pras, D. Schertl, M. Scholz, W. Traub, , G. Weigelt, and M. Wittkowski, "Observations of Mira stars with the IOTA interferometer," in *Proc. SPIE 4006: Interferometry in Optical Astronomy*, P. Lena and A. Quirrenbach, eds., SPIE, 2000.
4. P. Kervella, V. C. du Foresto, W. Traub, and M. Lacasse, "Cepheid observations by long-baseline interferometry with FLUOR/IOTA," in *Proc. SPIE 4006: Interferometry in Optical Astronomy*, P. Lena and A. Quirrenbach, eds., SPIE, 2000.
5. B. Mennesson, G. Perrin, G. Chagnon, V. C. du Foresto, S. Morel, C. Ruilier, W. Traub, N. Carleton, and M. Lacasse, "Thermal infrared stellar interferometry using single-mode guided optics: first scientific results on IOTA," in *Proc. SPIE 4006: Interferometry in Optical Astronomy*, P. Lena and A. Quirrenbach, eds., SPIE, 2000.
6. R. Millan-Gabet, F. Schloerb, and W. Traub, "Investigation of Herbig Ae/Be stars in the near-infrared with the IOTA," in *Proc. SPIE 4006: Interferometry in Optical Astronomy*, P. Lena and A. Quirrenbach, eds., SPIE, 2000.

7. S. Morel, W. Traub, J. Bregman, R. Mah, and E. Wilson, "Fringe-tracking experiments at the IOTA interferometer," in *Proc. SPIE 4006: Interferometry in Optical Astronomy*, P. Lena and A. Quirrenbach, eds., SPIE, 2000.
8. I. Porro, W. Traub, and N. Carleton, "Effect of telescope alignment on a stellar interferometer," *Applied Optics* **38**, pp. 6055–6067, 1999.
9. F. Malbet, P. Kern, I. Schanen-Duport, J.-P. Berger, K. Rousselet-Perraut, and P. Benech, "Integrated optics for astronomical interferometry," *Astron. Astrophys. Suppl.* **138**, pp. 135–145, 1999.
10. R. Millan-Gabet, F. P. Schloerb, W. A. Traub, and N. P. Carleton, "A NICMOS3 camera for fringe detection at the IOTA interferometer," *Publ.. Astron. Soc. Pac.* **111**, p. 238, 1999.

Fringe-tracking experiments at the IOTA interferometer

S. Morel[a], W. A. Traub[b], J. D. Bregman[c], R. Mah[c], and E. Wilson[c]

[a]Smithsonian Astrophysical Observatory - F. L. Whipple Observatory
670 Mount-Hopkins Road, Amado, AZ 85645, USA

[b]Smithsonian Astrophysical Observatory - Center for Astrophysics
60 Garden Street, Cambridge, MA 02138, USA

[c]NASA - Ames Research Center, MS 245-6
Moffet-Field, CA 94035, USA

ABSTRACT

The first tests of an infrared fringe-tracker prototype for the IOTA interferometer (Mount-Hopkins, Arizona) were carried out during 1999. The aim of this real-time system is to minimize the optical path difference (OPD) fluctuations between the two beams such that interference fringes (obtained in J, K, or L band) can always be observed within the "scan window" given by the instrument. After an introduction of the employed technology (hardware and software), we present results obtained from star observations. Finally, we discuss the possibility of improving the fringe-tracker by prediction of the OPD, using statistical properties of its fluctuations. The improvement of the fringe-tracker already existing for the FLUOR recombiner is discussed as well.

Keywords: fringe-tracking, coherencing, infrared detectors, precision positioning, prediction.

1. INTRODUCTION

A two-aperture stellar optical interferometer is always subject, while being operated, to variations of the optical path difference (OPD) between the two light beams coming from its telescopes. One of the OPD variation components is a deterministic signal related to the Earth's rotation. It is compensated by moving an optical delay line (ODL) according to a pointing model given by the declination of the observed object and its hour angle. The other components are random and are caused by atmospheric turbulence ("differential piston" mode of the turbulence), mechanical constraints, vibrations, and errors in the pointing model. Interference fringes are observable within an OPD interval roughly equal to the coherence length defined by $L_c = \bar{\lambda}^2/\Delta\lambda$, where $\bar{\lambda}$ is the mean filter wavelength and $\Delta\lambda$ is the spectral bandpass. Because of the random fluctuations in the OPD, during an observation the OPD is scanned on either side of the expected null-OPD point by a piezo-electric controlled mirror.

The aim of fringe-tracking is to perform a real-time correction of the length difference between the actual null-OPD position and the expected null-OPD position, in order to keep the fringes centered in the observing window. This difference is computed from the acquired fringe signal and is used to control an optical delaying device. In order to not "share the photons", the fringe-tracker uses the same data as for producing the "scientific" fringes, which are acquired for measuring source visibility points from the fringe contrast (imaging interferometry) or external delay (in case of astrometry by interferometry). However, in some cases, it may be useful to have separate recombiners for acquisition and tracking[1].

Further author information:

S.M.: E-mail: smorel@cfa.harvard.edu. Fax: 1 520 670 5751
W.A.T.: E-mail: wtraub@cfa.harvard.edu. Fax: 1 617 495 7105
J.D.B.: E-mail: jbregman@mail.arc.nasa.gov
R.M.: E-mail: rmah@mail.arc.nasa.gov
E.W.: E-mail: ed.wilson@ibm.net

Although it is possible to manually track the fringes (see part 3), significant fringe acquisition improvements are expected from an automatic fringe-tracker. The implementation of a fringe-tracker depends on the way fringes are acquired. With channeled spectra (for small apertures) or dispersed fringes (for apertures larger than Fried's parameter r_0) configurations, one can track fringes by respectively group-delay tracking[2] (GDT) or real-time active fringe tracking[3] (RAFT). This is done at visible wavelengths using photon-counting detectors. However, no photon-counting technology currently exists for the infrared: the fringe signal-to-noise ratio decreases with the number of pixels of the detector. The signal should be therefore "concentrated" on a minimal number of pixels. The classical "white-fringe" set-up is then employed (Fig. 1). The two beams are recombined by a beamsplitter. Fringes are acquired by linearly modulating (by a sawtooth signal ideally) the pathlength of one of the beams upstream from the recombination. Intensities of the recombined beams evolve therefore temporally as an interference fringe pattern. Due to reflections on the beamsplitter, there is a π phase-shift between the two interferometric signals obtained.

The pathlength scanned depends on the detector performances and is usually equal to a few coherence lengths. For a white-fringe set-up, one can perform "cophasing" in order to "freeze" fringes moved by atmospheric differential piston[4]. However, a very good fringe SNR is necessary for this technique. A less demanding way to perform fringe-tracking is called "coherencing": the OPD is corrected so that the fringes remain within the "observing window" defined by the scan length. Group-delay tracking and RAFT may be regarded as coherencing techniques. For any set-up, the OPD correction rate is between 0.2 Hz and 10 Hz. The duration of a cycle is therefore longer than the atmospheric τ_0.

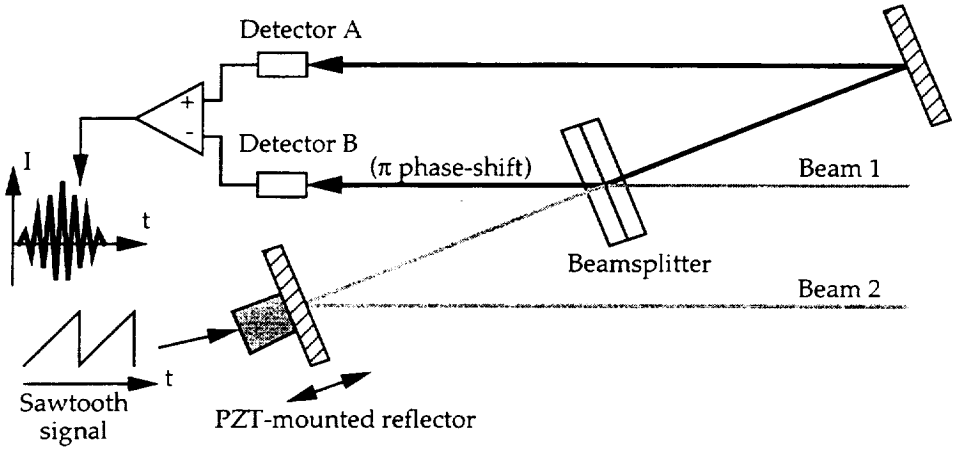

Figure 1. Schematic of a recombination table based on a beamsplitter, as it is employed at IOTA for fringe acquisition.

2. COHERENCING ALGORITHM

With a white-fringe set-up, the two interferometric signals resulting from a scan are subtracted to yield an interferogram. For each interferogram (or fringe packet) acquired, the computer performing fringe-tracking finds the null-OPD point and computes the offset to apply to the delaying device, in order to bring the null-OPD point to the center of the observing window (i.e., half-way along the scan length).

For IOTA (see part 3), a fringe packet scan consists of 256 temporally sampled points. Each value is a 16-bit integer. We use the following algorithm to find the null-OPD point in a fringe packet:

1) The photometric variations are removed by subtracting the local mean from each value of the fringe packet (computed from the values of the 20 points closest to a given point). An FFT bandpass filter can be used instead, and gives satisfactory results.
2) Any negative values in the scan are multiplied by -1 (equivalent to a rectifier bridge).
3) All the values that are not local maxima are set to zero.
4) Linear segments are interpolated between each pair of non-zero points (corresponding to the fringe peaks in the interferogram).

5) The resulting signal is smoothed by a "schematized" coherence envelope given by flat-top functions representing the main lobe and two sidelobes. The location of the maximum value in the signal resulting from the previous operation gives the null-OPD point.

These steps are illustrated in Fig. 2. This algorithm is actually a simplified version of one we developed that included phase measurement. The algorithm was first tested in the MatLab language using recorded interferograms, and showed good robustness to noise. Tests were also done using simulated interferograms: the RMS error on the null-OPD point found is never larger than 20 points. With the IOTA fringe acquisition system (see part 3), this corresponds to an error on the estimated null-OPD point of 8 μm, very good for a coherencing system.

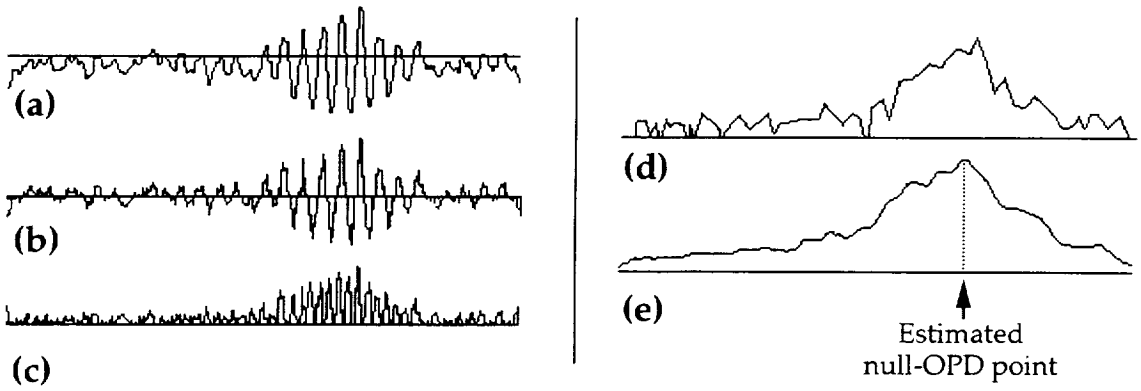

Figure 2. Illustration of the steps of the coherencing algorithm. (a): Interferogram acquired ; (b): signal obtained from this interferogram after step 1 (correction of the photometric variations) ; (c): signal obtained after step 2 (rectification) ; (d): signal obtained after steps 3 and 4 ; (d): signal obtained after step 5 (smoothing). The null-OPD point corresponds to the position of the maximum value in this signal.

3. FRINGE-TRACKER IMPLEMENTATION ON THE IOTA INFRARED TABLE

IOTA can currently use either a single-mode fiber recombiner called FLUOR[5] or a beamsplitter-based recombiner, as described in Fig. 1. For scanning the OPD, a plane mirror is mounted on a piezo-electric transducer (PZT) which is controlled by a triangle signal generated by a low-frequency analog function generator. Our fringe-tracker has been designed for this recombiner only. The detector used for fringe acquisition is based on a 256×256 pixel NICMOS III chip[6]. Only two pixels of this chip are read for acquiring interferometric signals. The maximum rate $f_s = 1/\tau_s$ is 10 interferograms per second, each one being 256 point wide. The NICMOS chip is controlled by signals generated by a 100 MHz Pentium PC which receives the sampled value of the addressed pixel. After processing, these values are sent to a Macintosh Quadra computer for displaying and recording the interferograms.

The delaying device used by IOTA for compensating the OPD due to Earth rotation is the "short ODL". It consists of a dihedral reflector mounted on an Anorad micro-positioning table. This table may be translated within a 2.3 m interval by 10 nm steps thanks to an electric linear motor featuring a laser metrology based position servo-loop. The short ODL is controlled by another Macintosh Quadra. Without fringe-tracking, the operator has to check the position of the interferogram displayed by the first Quadra and manually modify the short ODL position from the second Quadra to keep the fringe packet observable. This operation is difficult when there is significant atmospheric turbulence. Implementing an automatic coherencer fringe-tracking system would therefore significantly improve data acquisition on IOTA.

To implement the fringe-tracker, the algorithm described in part 2 was coded in the C++ language on a temporary Macintosh PowerBook (100 MHz PowerPC CPU). The interferogram acquisition and ODL control programs were modified to communicate with the fringe-tracker computer: each interferogram is sent through the Ethernet local area network (LAN) of IOTA to the fringe-tracker. After having found the null-OPD point in the interferogram, the fringe-tracker computer sends the OPD correction to the ODL control computer which adjusts the short ODL position.

The test of this first version of the IOTA fringe-tracker consisted of observing bright stars such as ι-Aur or β-Gem. Some problems, related to the design of the fringe-tracker were detected. The TCP/IP protocol used for communication between the computers is not suitable for our real-time application involving MacOS computers. Hence, we now use UDP (User Datagram Protocol) which is a socket-based protocol faster and more flexible than TCP/IP, for all the IOTA applications requiring inter-communication by LAN. For example, the long-ODL is managed by a Linux computer located at the north end of the IOTA baseline. This computer is commanded from the Quadra controling ODLs via UDP. A second problem was that at the higher scan rates (10 Hz), the inertia of the short-ODL was too large to allow it to respond to the tracking commands.

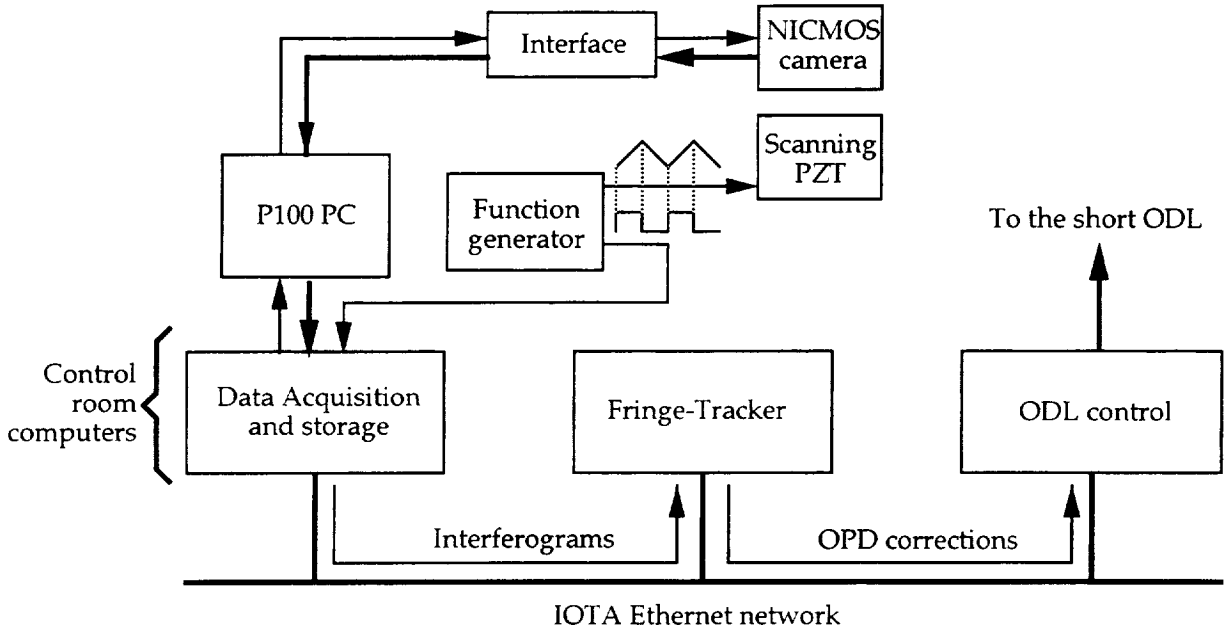

Figure 3. Diagram of the data flow in the fringe-tracking system tested on IOTA.

4. WHAT REMAINS TO BE DONE

4.1 PZT control

The scanning PZT is driven by a Physik Instrumente high-voltage amplifier featuring a function generator programmable by an external computer. All the parameters which control the generated signal are sent through a serial link to the amplifier. It will therefore be possible to reduce the scan range (i.e. slowing down the velocity of the scanning mirror while keeping the same sampling rate) to increase the fringe SNR if the differential piston is not too large. In this case, the high frequency OPD corrections would be directly applied to the scanning PZT by adding an voltage offset to the driving signal. The lower frequency OPD errors, which can exceed the range of the PZT, would be corrected by using the short ODL to bring the PZT back to the middle of its mechanical range (which should correspond to the null-OPD point). Moreover, the duty-cycle of the signal can be modified to increase the efficiency of the acquisition system.

Controlling the PZT requires a device to synchronize the NICMOS acquisition. In the current IOTA control system, acquisitions by the Quadra are triggered by the leading edge of a TTL signal delivered by the external function generator. This TTL signal is synchronized with the triangle signal driving the PZT. For the fringe-tracker using PZT control, we wired an electronic temporal derivator giving a rectangular signal from the signal delivered by the amplifier.

However, the IOTA control system should be soon replaced by a VME chassis with PowerPC boards running under Wind-River's VxWorks, a real-time operating system[7]. Many improvements are expected from this new system which will control siderostat and ODL motion, tip-tilt correction and fringe acquisition. The implementation of a fringe-tracker will be easier thanks to a simplification of the communication between the processes.

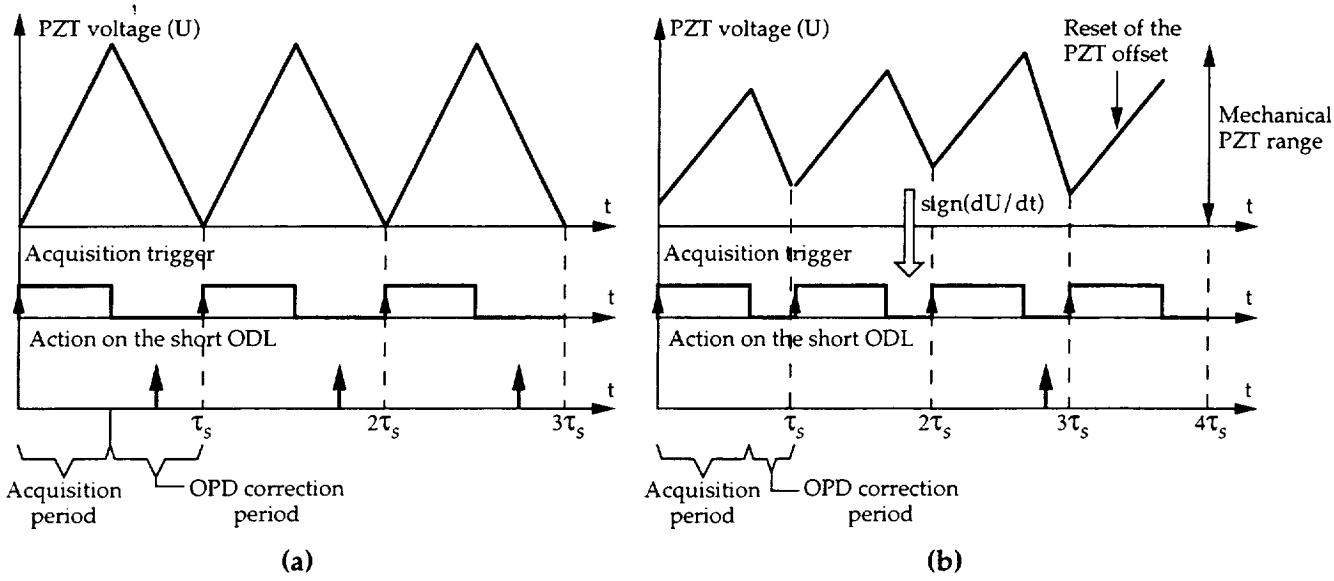

Figure 4. Chronograms of the voltage applied to the scanning PZT, the corresponding TTL signal for triggering NICMOS acquisitions, and the OPD correction on the short optical delay-line. (a): current situation ; (b): future system with PZT control by the fringe-tracker.

4.2 Prediction of the null-OPD point

Although the atmospheric differential piston is a random signal, its statistical properties are described by Tatarski's models. Let ΔL_{dp} be the OPD component related to the differential piston for an interferometer characterized by a projected baseline B and apertures of diameter equal to D. From Taylor's hypothesis of a frozen turbulence moving at velocity V_a (with $\mathbf{B} = k.\mathbf{V}_a$), the power spectrum of ΔL_{dp} can be modeled by[8]:

$$\begin{cases} \mathcal{W}_{\Delta L_{dp}}(f) \propto f^{-2/3} & ; \quad \text{if } f < \dfrac{\mathrm{V}_a}{2\mathrm{B}} \\ \mathcal{W}_{\Delta L_{dp}}(f) \propto f^{-8/3} & ; \quad \text{if } \dfrac{\mathrm{V}_a}{2\mathrm{B}} \leq f < \dfrac{0.3\mathrm{V}_a}{D} \\ \mathcal{W}_{\Delta L_{dp}}(f) \propto f^{-17/3} & ; \quad \text{if } f \geq \dfrac{0.3\mathrm{V}_a}{D} \end{cases} \tag{1}$$

This power spectrum indicates that the temporal autocorrelation of ΔL_{dp} is not equal to zero for $\tau \neq 0$ (τ being the argument of the autocorrelation function), i.e. ΔL_{dp} is not white-noise. We assume that only the atmospheric differential piston significantly modifies the position of the null-OPD point from one scan to the next one. The signal measured by the fringe-tracker is:

$$s[n] = \Delta L_{dp}[n] - \Delta L_{dp}[n-1] = \Delta L[n] - \Delta L[n-1], \tag{2}$$

where n is an integer indexing the values of ΔL_{dp} for each scan. ΔL can be tracked from an origin by integrating s, yielding a temporal signal u. The fact that u, reflecting ΔL_{dp}, is temporally autocorrelated has been proved by using the first version of the fringe-tracker in open loop and measuring u for each scan from the position of the null-OPD point. The autocorrelation of u has then been computed yielding the result illustrated in Fig. 5. u can therefore be described by the auto-regressive (AR) model:

$$\tilde{u}[n+1] = \sum_{i=0}^{P-1} a[i].u[n-i], \tag{3}$$

where P is the order of the model. The issue is to determine the values of the AR model $\underline{a} = (a_0, ..., a_{P-1})^{\mathrm{T}}$ to minimize the mean quadratic error $< |u[n] - \tilde{u}[n]|^2 >$. Since no assumption regarding the stability of u can

be made, especially for long observing periods where the turbulence conditions are changing, one should use an adaptive method to correct the AR model at each step, according to the actual value of u (determinated from the algorithm described in part 2). We propose to use the weigthed recursive least square algorithm (WRLS), a familiar signal-processing method. At each scan indexed by n, the expected OPD is computed from the following equations:

$$\begin{cases} \underline{K}[n+1] = \underline{V}[n].\underline{u}[n].(\Lambda + \underline{u}[n]^{\mathrm{T}}.\underline{V}[n].\underline{u}[n])^{-1} \\ \underline{V}[n+1] = (\underline{1} - K[n+1].u[n]^{\mathrm{T}}).\underline{V}[n].\Lambda^{-1} \\ \underline{a}[n+1] = \underline{a}[n] + \underline{K}[n+1].(u[n+1] - \underline{a}[n]^{\mathrm{T}}.\underline{u}[n]) \end{cases} , \tag{4}$$

where $\underline{K}$ is a vector representing the adaptation gain (or "Kalman gain"), $\underline{V}$ is the covariance matrix, $\underline{1}$ is the identity matrix, $\underline{u}[n] = (u[n], ..., u[n-P-1])^{\mathrm{T}}$, and Λ is the "forgetting factor" used to accelerate the convergence of the AR model. Usually, $0.8 < \Lambda < 1$. This algorithm has already been proposed to improve fringe-tracking with GDT or RAFT[9]. Methods of the same type using ARMA models have been successfully used for adaptive optics[10]. In the case of IOTA, prediction could be employed for enhancing tip-tilt correction as well.

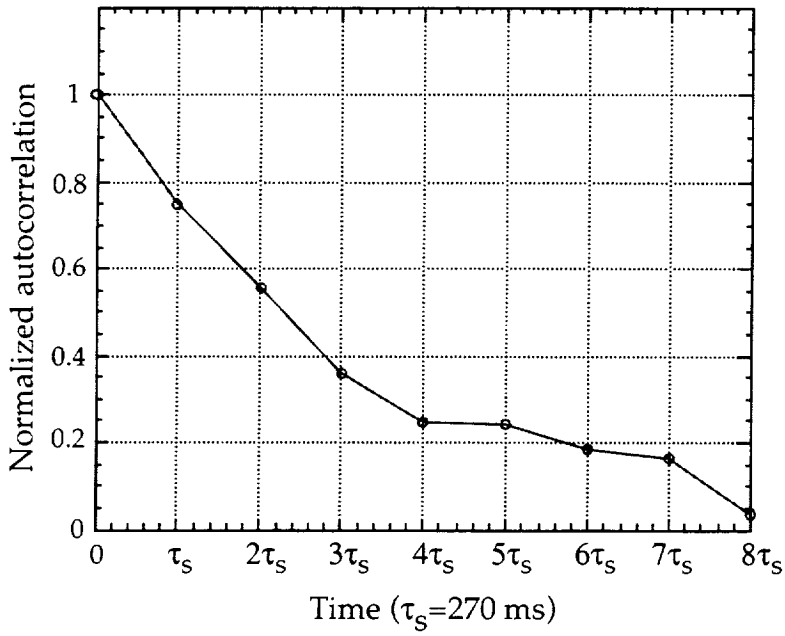

Figure 5. Normalized discrete temporal autocorrelation of the optical path difference drift (from a reference point) measured at IOTA with a 38 m baseline.

4.3 Fringe-tracking with FLUOR

The FLUOR recombiner has recently been improved and yields very accurate fringe contrast measurements. Its control system consists of a Macintosh G3 400 MHz computer in charge of NICMOS acquisition, scanning-PZT control (different from the one used on the beamsplitter table), and short-ODL control. The whole control software has been developed with National Instruments' LabVIEW graphic language. Thanks to this compact system and to the low scan rate used (2 Hz max.), a coherencer has easily been implemented on the FLUOR control system. It consists of finding the position of the centroid in the fringe packet. Each fringe packet has previously been filtered through a bandpass filter. Then, the mean of the raw fringe packet is added to the previous filtered signal to yield the final fringe packet to analyze. The OPD is corrected by moving the short-ODL. The FLUOR coherencer features an automatic fringe detector triggered when there is, in the interferogram, at least one peak whose amplitude is larger than a pre-set threshold. However, this detector may be deceived by "light-bursts", which sometimes occur in a fringe-packet. Detecting peaks at different bandwidths should eliminate this problem.

Since FLUOR is intended to be more heavily used on IOTA, it would be interesting to try to improve the FLUOR coherencer by using the algorithm described in part 2 and/or the prediction algorithm. Tests should be

carried out during year 2000. However, first tests of the coherencer algorithm applied to FLUOR have recently been done. For "clean" fringes with high SNR (obtained by observing π-Leo with the 38-meter baseline of IOTA) and good turbulence conditions, no significant difference between our algorithm and the centroid method appeared. In both cases, with a 2 Hz scan rate, the standard deviation of the residual OPD (difference between the measured null-OPD point and the center of the scan window) was $\sigma = 14\,\mu$m.

5. CONCLUSION

An automatic coherencing system for an infrared stellar interferometer can be made from a simple and fast algorithm. However, its implementation strongly depends on the characteristics of the existing control system. It is optimal to have only one computer in charge of fringe acquisition, null-OPD point measurement, and OPD correction. For IOTA, the current coherencer algorithm will normally used for the beamsplitter table during all observations once the new VxWorks system is installed. Then, prediction algorithms will be added to try to improve the performance of this coherencer. This might also benefit the FLUOR coherencer which already exists. New improved algorithms for measuring the null-OPD point in a fringe packet with a better accuracy are currently being studied. Closure-phase experiments at IOTA (scheduled for 2001) will certainly require such a coherencing system.

6. ACKNOWLEDGEMENTS

We thank M. G. Lacasse for his help during the fringe-tracker experiments at IOTA. We also thank V. Coudé du Foresto and G. Perrin for having helped us to use the FLUOR recombiner. S. Morel is grateful to DGA-DRET (the scientific research office of the French Ministry of Defense) which funded him in 1999, and to NASA and the Smithsonian Institution for his year 2000 fellowship.

7. REFERENCES

1. J. T. Armstrong, D. Mozurkewich, T. A. Pauls, A. R. Hajian, "Bootstrapping the NPOI: keeping long baselines in phase by tracking fringes on short baselines", *Proceedings SPIE, 'Astronomical Interferometry', 20-27 March 1998, Kona, Hawaii*, **3350**, pp. 461-466, 1998.
2. P. R. Lawson, "Group-delay tracking in optical stellar interferometry with the fast Fourier transform", *J. Opt. Soc. Am.* **A 12**, pp. 366-374, 1995.
3. L. Koechlin, P. R. Lawson, D. Mourard, A. Blazit, D. Bonneau, F. Morand, Ph. Stee, I.Tallon-Bosc, F.Vakili, "Dispersed fringe tracking with the multi-r_0 apertures of the Grand Interféromètre à 2 Télescopes", *Appl. Opt.* **35**, pp. 3002-3009, 1996.
4. M. Shao, D. H. Staelin, "Long-baseline optical interferometer for astrometry", *J. Opt. Soc. Am.* **67**, pp. 81-86, 1977.
5. V. Coudé du Foresto, G. Perrin, C. Ruilier, B. Mennesson, W. A. Traub, M. G. Lacasse, "FLUOR fibered instrument at the IOTA interferometer", *Proceedings SPIE, 'Astronomical Interferometry', 20-27 March 1998, Kona, Hawaii*, **3350**, pp. 856-863, 1999.
6. R. Millan-Gabet, F. P. Schloerb, W. A. Traub, N. P. Carleton, "A NICMOS3 camera for fringe detection at the IOTA interferometer", *Publ. Astron. Soc. Pac.* **111**, pp. 238-245, 1999.
7. W. A. Traub, N. P. Carleton, J. D. Bregman, M. K. Brewer, M. G. Lacasse, P. Maymounkov, R. Millan-Gabet, S. Morel, C. Papaliolios, M. R. Pearlman, I. Porro, F. P. Schloerb, "The third telescope project at the IOTA interferometer", *Proceedings SPIE, 'Interferometry in Optical Astronomy', 27-31 March 2000, Munich, Germany*, **4006**, in preparation.
8. G. Perrin, "Correction of the "piston effect" in optical astronomical interferometry. I. Modulus and phase gradient of the visibility function restoration", *Astron. & Astroph. Suppl. Ser.* **121**, pp. 553-568, 1997.
9. S. Morel, L. Koechlin, "Fringe tracking using a priori information on the optical path difference drift", *Proceedings SPIE, 'Astronomical Interferometry', 20-27 March 1998, Kona, Hawaii*, **3350**, pp. 1057-1064, 1998.
10. C. Dessenne, P.-Y. Madec, G. Rousset, "Optimization of a predictive controller for closed-loop adaptive optics", *Appl. Opt.* **37**, pp. 4623-4633, 1998.